Eur. Phys. J. B **56**, 15–26 (2007)
DOI: 10.1140/epjb/e2007-00085-7

THE EUROPEAN PHYSICAL JOURNAL B

Front roughening in three-dimensional imbibition

M. Dubé[1], C. Daneault[1], V. Vuorinen[2], M. Alava[2], and M. Rost[3,a]

[1] Centre de Recherche en Pâtes et Papiers, Université du Québec à Trois-Rivières, C.P. 500, Trois-Rivières, Québec, G9A 5H7, Canada
[2] Laboratory of Physics, Helsinki University of Technology, P.O. Box 1100, 02015 HUT, Finland
[3] Abteilung Theoretische Biologie, IZMB, Universität Bonn, Kirschallee 1, 53115 Bonn, Germany

Received 16 March 2007 / Received in final form 13 February 2007
Published online 28 March 2007 –

Abstract. We investigate the structure and dynamics of the interface between two immiscible liquids in a three-dimensional disordered porous medium. We apply a phase-field model that includes explicitly disorder and discuss both spontaneous and forced imbibition. The structure of the interface is dominated by a length scale $\xi_\times$ which arises from liquid conservation. We further show that disorder in the capillary and permeability act on different length scales and give rise to different scalings and structures of the interface properties. We conclude with a range of applications.

PACS. 46.55.+d Tribology and mechanical contacts – 81.40.Pq Friction, lubrication, and wear – 07.79.-v Scanning probe microscopes and components – 83.50.Lh Slip boundary effects (interfacial and free surface flows)

1 Introduction

The flow of fluids through a porous medium has a tremendous importance in fields as diverse as the petroleum industry [1], the pulp and paper science [2–5], in soil science [6] and the construction industry [7,8]. Particularly important for pulp and paper are ink penetration into paper, and its relation to printing defects [3], water evaporation from a freshly formed sheet, and surface coating [4,5]. Of similar interest in soil science is contaminant infiltration and sedimentation [9,10].

Despite this importance, several aspects of the flow remain unknown and the problem poses several challenges, both theoretical and experimental [11]. This is in part due to the fact that widely diverse length and time scales are present. The flow of liquids depends on the physics at the pore level (of length of a few μm or less) while the observable effects extend from lengths of a few cm up to several meters. Likewise, the invasion of a single pore may occur on the scale of a millisecond while the complete absorption process may range from a few seconds to several minutes or even hours. The problem is thus to connect these length and time scales in a satisfactory way. Empirical relations to describe both single and multiphase flow of liquids through a porous medium have existed for a long time, but it is only recently that qualitative and quantitative knowledge of the flow has been gained [6,12–15].

A crucial aspect of the flow pattern is that it is never homogeneous; the disordered pore structure leads to uneven flow. In the case of multiphase flows with immiscible liquids, this is reflected in the shape of the interface separating them. Typically, the interface is not flat but presents a rough, stochastic structure, as depicted in Figure 1. In some cases, the interface can even be unstable, leading to the formation of discontinuous domains [12]. It is clear that an unstable interface can have severe consequences, e.g., in oil recovery, and several studies have tackled this problem, within percolation theory and detailed network simulations [12,16,17]. Even if the the interface is stable, its stochastic nature has several observable effects. For example, solid particles or chemicals are often carried by the flow (hydrodynamic dispersion [13]). These can be pollutants in ground-water flow or ink pigments during the printing process. The inhomogeneities of the flow are then reflected in the distribution of pollutants or ink pigments. For ink in paper, this uneven ink penetration leads to the formation of a print defect called "mottle" [18]. Another example of the effect of uneven fluid flow is provided in Figure 2, which shows light transmission across a sheet of a dry paper as it is imbibing water.

Our purpose in this paper is to describe the structure and the dynamics of a rough interface between two fluid phases in a three-dimensional porous medium during the process of imbibition. We discuss the case illustrated in Figure 1 where the medium, originally dry or saturated with another fluid, is immersed into a reservoir. The imbibition process can either be spontaneous, due solely to capillary forces, or be forced at some volume rate of flow. We concentrate on cases where the imbibition

[a] e-mail: martin.rost@uni-bonn.de

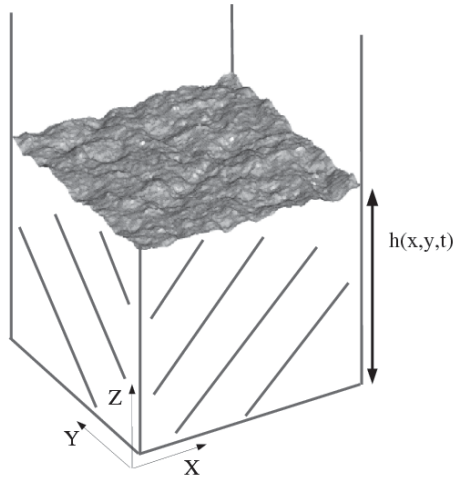

Fig. 1. Schematic representation of the imbibition process. The three-dimensional porous medium is in contact with a liquid reservoir at $z = 0$ and a rough interface $h(\mathbf{x}, t)$ between the wet and dry part of the medium evolves dynamically. The imbibition process can be either spontaneous or forced.

front remains compact, in which case an interface separating the wet and non-wet part of the medium exists and is denoted by the position $h(\mathbf{x}, t)$ where $\mathbf{x} = (x, y)$ are the spatial coordinates in the transverse plane. This situation was also considered by Tartakosvky et al. [14], who have shown that the randomness of the front increased in time. Similar fluctuations in the interface were shown by Ronen et al. [15] to be essential to an understanding of the phenomenon of capillary fringe in porous media. To treat this case, we introduce a phase-field model that includes explicitly surface tension, liquid conservation as well as disorder, both at the level of the capillary pressure and permeability. We show that the interface is a self-affine fractal which can be described within the framework of dynamical roughening and scaling [19]. We discuss the consequences of the imbibition dynamics for the "unevenness" of the imbibed liquid in relation to typical industrial operations, as illustrated, e.g., in by Figure 2. A brief account of these results has been published in reference [20], with specific applications to printing phenomena. Here, we expand and generalize the model, present new results on the effect of permeability disorder and on the temporal behavior of the interface roughness (including pinning by gravity) and consider a broader range of possible applications.

We consider the case where a viscous liquid displaces a gas or another liquid with a much smaller viscosity. In this case, the flow is characterized by the viscosity η of the imbibing fluid and the surface tension σ of the interface between the fluid and the other fluid/gas. The main quantities characterizing the porous medium are the coarse-grained permeability κ and the capillary pressure p_c. The permeability describes the ease with which a fluid can flow through the medium while the capillary pressure describes the "suction" property of the medium. The fluid flow is inhomogeneous due to the disordered structure of

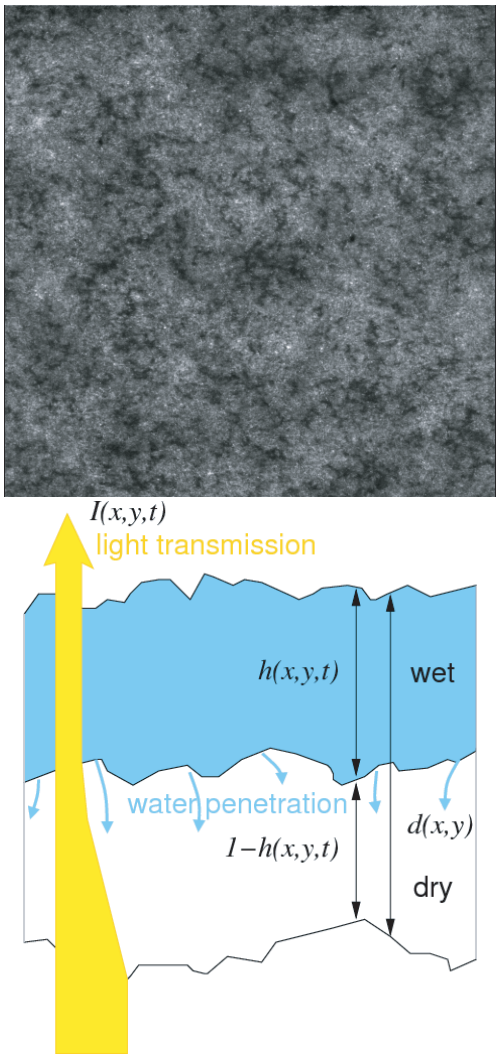

Fig. 2. Top view of light transmission through a sheet of paper with water penetrating from the bottom towards the top. The sheet, with non-uniform thickness $d(\mathbf{x})$ is lit from below with visible light, which allows a good resolution. The wet sheet scatters light less strongly than the dry sheet and points of high intensity then correspond to high local values of $h(\mathbf{x}, t)$. In a first approximation, the intensity of light through the sheet $I(\mathbf{x}, t) = I_0(\mathbf{x}) \exp(\gamma h(\mathbf{x}, t))$ where $I_0(\mathbf{x})$ is the initial (before wetting) intensity of transmitted light and $h(\mathbf{x}, t)$ is the height of the invasion front.

the medium. In terms of macroscopic quantities, this disorder is reflected into variations $\Delta\kappa$ and Δp_c of the permeability and capillary pressure respectively. We shall show that the controlling parameter of the roughening process is the capillary number

$$Ca = \frac{\eta v}{\sigma} \tag{1}$$

where v is the velocity of the flow, and that the relative importance of capillary and permeability disorder is characterized by a length scale

$$\xi_\kappa = \frac{\sqrt{\kappa}}{Ca}. \tag{2}$$

Note that by its definition κ has a dimension of area or length squared. On length scales much smaller than ξ_κ, roughening is dominated by capillary disorder while permeability disorder is relevant at large length scales. We further show that there exists a length scale

$$\xi_\times = \sqrt{\frac{\kappa}{Ca}} \tag{3}$$

which arises from the conserved nature of the fluid. This length scale separates two regimes of roughness; at low capillary numbers and in spontaneous imbibition, the front has the roughness exponent $\chi = 0.75$ on length scales $l \ll \xi_\times$ and is asymptotically flat for $l \gg \xi_\times$. The ratio of the two length scales $\xi_\kappa/\xi_\times = Ca^{-1/2}$ which means that short length scale roughness is dominated by capillary disorder in typical situations ($Ca < 1$). In cases where the disorder in the permeability is present and dominant, the short scale ($l \ll \xi_\times$) roughness has an exponent $\chi = 3/2$ while being flat asymptotically. In general however, capillary disorder is dominant.

The outline of this paper is as follows. In the next section, we describe pattern formation in imbibition, specify the conditions under which a sharp rough interface exists between the two fluids and briefly describe the concepts of dynamical scaling. We also introduce the phase field model of imbibition, list the conditions under which it can be applied and connect the model with phenomenological interface equations. Section 3 presents the results of the numerical simulations. We discuss separately spontaneous and forced imbibition and highlight the role of disorder in the permeability. Applications of the results as well as the conclusions are presented in Section 5.

2 Fluid flow in disordered media

The flow of the liquids is influenced in great part by the surface chemistry of the underlying solid matrix, which is reflected in their wettability properties, and in the contact angle θ which determines whether a liquid is wetting or non-wetting. Important is also σ, the surface tension associated with the interface between the wetting and non-wetting liquids. In a pore of radius R_0, the combination of the curved interface and surface tension creates a pressure difference or capillary pressure

$$\Delta p \equiv p_c = 2\frac{\sigma\cos\theta}{R_0} \tag{4}$$

which gives rise to the motion of the fluids.

Imbibition refers to the case where the wetting fluid displaces the non-wetting one, while the opposite case is called drainage. Spontaneous imbibition occurs when the invading fluid does so under the sole influence of capillary forces, with no external pressure while forced imbibition involves a combination of capillary phenomena and an externally enforced flow rate or pressure difference.

The fluids are characterized by the viscosity, η_i and density ρ_i where $i = w, nw$ refers respectively to the wetting and non-wetting fluids; the viscosity ratio is $M = \eta_w/\eta_{nw}$. The study of flows in specifically designed porous networks has been used to observe several microscopic mechanisms for fluid flow. The most important are film flow along the solid matrix (pore walls) and piston-like motion of the fluid [11]. Depending on the relative importance of these mechanisms, several phenomena can be observed [12]. There can be discontinuous formation of wetted domains due to *surface flow* in pores, of branched structures, as well as compact domains with well defined interfaces.

The controlling parameters are the viscosity ratio M of the two fluids and the capillary number, equation (1). For $M \gg 1$ and large enough capillary numbers a sharp rough interface exists, with a spatial structure presenting stochastic fluctuations similar to those represented in Figure 1.

These fluctuations belong to the field of kinetic roughening, which has a long history [19]. For the special case of imbibition we refer to [11] and give a brief overview here. Statistical properties of interface configurations are extracted from ensemble averages over different realizations of disorder (denoted by brackets $\langle\rangle$) and spatial averages (denoted by an overbar). These yield the average height

$$H(t) = \langle\overline{h(\mathbf{x},t)}\rangle, \tag{5}$$

and it is useful to note that in contrast to many other phenomena, in spontaneous imbibition $H(t)$ does not increase with a constant velocity. The roughness of the interface is described by the total variance or square of its width $w^2(t) = \langle\overline{(h(\mathbf{x},t) - H(t))^2}\rangle$, and the related spatial height-difference correlation function $G(\mathbf{x},t) = \langle\overline{(h(\mathbf{x}+\mathbf{x}',t) - h(\mathbf{x}',t))^2}\rangle^{1/2}$. Usually more convenient is the structure factor $S(\mathbf{k},t) = \langle|h(\mathbf{k},t)|^2\rangle$ calculated from the Fourier transform $h(\mathbf{k},t)$ of the interface profile. For isotropic media $S(\mathbf{k},t) = S(k,t)$ with $k = |\mathbf{k}|$. The total variance of the interface is related to the structure factor by

$$w^2(t) = 2\pi\int dk\; kS(k,t). \tag{6}$$

Self-affine rough interfaces exhibit scaling forms of these quantities. The vertical extent of amplitude fluctuations $w(t)$ depends on their lateral correlation length $\xi(t) \sim t^{1/z}$ by the relation $w(t) \sim \xi(t)^\chi$.

In the present case, we expect the frozen-in quenched nature of the noise to be dominant. In such cases, usually the roughness falls either into the Quenched Edwards-Wilkinson (QEW) or Directed Percolation Depinning (DPD) universality classes. The QEW universality class is appropriate for domain walls in disordered magnets and was also shown to be partly relevant in imbibition of thin porous media. For a two-dimensional interface, a numerical determination of the exponents yields $\chi = 0.75$ [21,22]. The DPD universality class was originally designed specifically to model imbibition, but its application remains inconclusive up to now. For a two dimensional interface, the scaling exponent under DPD roughening is $\chi \simeq 0.4$ [19,24,23].

2.1 Phase field model of imbibition

Empirical descriptions of fluid flow in porous media are based on Darcy's law, which relates the flux of liquid to a macroscopic pressure gradient

$$\mathbf{j} = -\frac{\kappa}{\eta}\,\boldsymbol{\nabla} p \tag{7}$$

as well as viscosity and permeability of a given material. This equation is valid at the level of a representative volume element [25], and although it can be modified in case of film flow [26], due to inertial effects [27], or swelling of the porous matrix [28], it is generally a valid description of the flow.

For multi-phase flow of incompressible fluids, the dimensionless saturations of wetting and non-wetting fluids c_w and c_n are defined as their respective volume fractions. These are proportional to the concentrations, $\rho_i = \mathcal{P} c_i$, where $\mathcal{P}$ is the porosity. By liquid conservation the dynamics of the fluids is then obtained through continuity equations. For constant porosity

$$\begin{aligned} \frac{\partial \rho_w}{\partial t} + \boldsymbol{\nabla}\cdot\mathbf{j}_w &= 0 \\ \frac{\partial \rho_n}{\partial t} + \boldsymbol{\nabla}\cdot\mathbf{j}_n &= 0 \end{aligned} \tag{8}$$

together with the constraint $\rho_w + \rho_n = \mathcal{P}^{-1}$. The flux $\mathbf{j}_i$ of each fluid obeys equation (7) and a closure relation between the pressures in the two fluids $P_w - P_n = p_c$ at the interface introduces a *coarse-grained* capillary pressure, cf. equation (4).

Since the permeability is only a geometric factor, both fluids should have identical values of κ. We neglect that trapped droplets of the receding fluid or similar blocking mechanisms as well as swelling of the surrounding matrix may lead to a dependence of the permeability on the respective saturations, $\kappa_i = \kappa_i(c_w)$, because in most parts the c_i are either 0 or 1 and we consider the eventual value of κ_i at those saturations.

A particular case of equation (8) is when the non-wetting fluid cannot support a pressure gradient and has no intrinsic dynamics. This is the case examined in this paper and is often described using Richard's Equation [29]

$$\frac{\partial \rho}{\partial t} = \boldsymbol{\nabla}\cdot(D(\rho)\boldsymbol{\nabla}\rho) \tag{9}$$

where $D(\rho) = \eta^{-1}\kappa(\rho)\ \partial p_c(\rho)/\partial\rho$ is a phenomenological diffusion constant. This phenomenological approach is not useful to study front roughening since spatial non-homogeneities in the capillary pressure and permeability are not explicitly included. It also misses the crucial role of the front in the fluid intake.

The role of a roughening front can be explored by simulations based on percolation theory [30,31] or using detailed pipe network models [32]. The former applies very well when the flux of liquids are extremely small, but cannot deal entirely with the situation at hand since liquid conservation is not included. Pipe network models explicitly include conservation and thus serve to explore front instability and to obtain the curves of concentration-dependent permeability and capillary pressure. They are however computationally very heavy, and cannot deal easily with front roughening.

A continuum approach, based on phase-fields, was taken by Dubé et al. and Hernández-Machado et al. [33–37], as well as Mitkov et al. [38] and Papatzacos [39]. This approach is different from those based on interface equations, as it concentrates on the bulk of the porous medium, into which is incorporated disorder. It is a coarse-grained mesoscopic approach which includes automatically the relevant interface equation. It is also possible to obtain approximate interface equations for the front roughness. Even though these may not reproduce exactly all scaling exponents, the procedure highlights the relevant length scales of the problem.

The simplest phase field approach to imbibition starts from the observation that all coarse-grained descriptions of flow in porous media, based on Darcy's Law equation (7), are essentially diffusive (the presence of the viscosity results already from the coarse-graining procedure). So all inertial effects of hydrodynamics are neglected and only the pressure gradient determines the flux of liquid $\mathbf{j}$.

The fluid saturation $c(\mathbf{r},t)$ ($\mathbf{r} = (\mathbf{x}, z)$) is then defined throughout the column of the porous medium, with dynamical evolution of equation (8) for the wetting fluid. The flux is taken to be of Darcy's form, $\mathbf{j} = -\eta^{-1}\kappa(\mathbf{r},c)\nabla p$, with a permeability that may be a function of both space and concentration. However, the interface between the fluid and air should also appear explicitly, since this is where the capillary pressure arises.

This is accomplished by introducing a generalized thermodynamic free energy for the saturation field

$$F[c] = \int d\mathbf{r}\left(\frac{1}{2\beta}c^2(c-1)^2 - g(c)p_c(\mathbf{r}) + \frac{K}{2}|\boldsymbol{\nabla} c|^2\right). \tag{10}$$

To obtain the corresponding Cahn-Hilliard equation one derives the corresponding chemical potential which corresponds to the *pressure* in the porous medium because it drives the flux,

$$P(c,\mathbf{r}) = \beta^{-1}c(c-1)(2\,c-1) - K\nabla^2 c - g'(c)\ p_c(\mathbf{r}) \tag{11}$$

where β is the compressibility of the fluid [40] and K is a constant related to the effective interface tension between both fluids. Strictly speaking, the model should include both concentration and density as variable, with associated chemical potential and pressure [11,35]. However, in the present case of an incompressible fluid displacing a non-wetting fluid (whose dynamics is essentially irrelevant in the situation where the interface remains compact) the pressure and chemical potential are trivially related and the present description is perfectly adequate.

For $p_c = 0$, this free energy allows two stable homogeneous phases, described by the values $c = 1$ and 0, which we interpret as liquid and air respectively. Variations in the concentrations are penalized by the presence of the square gradient term but this term also allows a solution

that connects the liquid and air phase,

$$c(z) = \frac{1}{2}\left(1 + \tanh\frac{z - z_0}{\zeta}\right) \tag{12}$$

in the direction perpendicular to the interface. This solution describes an interface of finite thickness $\zeta \sim (\beta K)^{1/2}$ located at $z = z_0$ between homogeneous regions of saturation $c = 1$ and $c = 0$. With this interface is associated a surface tension $\sigma = (K/\beta)^{1/2}$ which corresponds to the energy increase brought by the interface. This is a phenomenological coarse-grained surface tension that does not necessarily correspond to the microscopic surface tension in a pore. It is present whenever there is contact between fluid elements in adjoint pores and acts in a way that minimizes the global liquid-air interface.

The term $g'(c) = dg(c)/dc$ is chosen so that it is nonzero only within the interfacial region and p_c thus corresponds to a coarse-grained capillary pressure. For convenience, we choose $g(c) = c^2(3-2c)/6$, so that $g'(c) = c(1-c)$, but the precise form of this term is not relevant.

The role of pressure is also apparent in the boundary conditions [33]. In the case of spontaneous imbibition the pressure at the bottom of the medium is set to the atmospheric pressure $p(\mathbf{x}, z = 0) = p_0$. The boundary condition at the upper end $\partial_z p(\mathbf{x}, z = L_z) = 0$ ensures that there are no pressure gradients on top of the porous medium. These lead to boundary conditions on the saturation $\partial_z c(\mathbf{x}, z = L_z) = 0$ and at $z = 0$ a value c solving

$$\beta^{-1} c\,(c-1)(2c-1) - p_c = 0. \tag{13}$$

In order to model imbibition situations at constant flow rate, as in [41], constant flux boundary conditions $\kappa\,\partial_z p = \eta\gamma_0$ are imposed. Both situations, spontaneous imbibition and constant flux shall be examined in details below.

Gravity stops the imbibition front at a height where capillary and hydrostatic pressure balance and produces a pinned interface. This can be taken into account by adding the hydrostatic component $p \to p - \rho_{\mathrm{m}} g c(\mathbf{r}) z$ where ρ_{m} is the fluid mass density and g is the gravitational constant. Inserting the pressure into the continuity equation for the wetting fluid, equation (8) yields an imbibition model of the form [36]

$$\eta\,\frac{\partial c(\mathbf{r},t)}{dt} - \rho g \frac{\partial \kappa(c,\mathbf{r}) c(\mathbf{r},t)}{\partial z} = \boldsymbol{\nabla}\cdot(\kappa(c,\mathbf{r})\nabla p). \tag{14}$$

Note that although gravity can only be introduced properly through an hydrodynamical field [42], the convective term reproduces the correct equation of motion for the average position of the imbibition front.

Disorder enters the problem naturally though the transport properties of the porous medium. The capillary pressure can change throughout the medium and so we assume the following correlations

$$\begin{aligned} \langle p_c(\mathbf{r})\rangle &= \bar{p}_c > 0 \\ \langle p_c(\mathbf{r}) p_c(\mathbf{r}')\rangle - \bar{p}_c^2 &= (\Delta p_c)^2 \delta(\mathbf{r}-\mathbf{r}'). \end{aligned} \tag{15}$$

Gaussian distribution is assumed, but the results do not depend on the precise shape of distribution, only on the first and second moments quoted above because the phase field effectively averages over regions of size ζ^3. The local permeability, $\kappa(\mathbf{r})$ (neglecting any dependence on the fluid saturation c) is also assumed random, characterized by the correlations (again the precise shape of distribution does not matter)

$$\begin{aligned} \langle \kappa(\mathbf{r})\rangle &= \bar{\kappa} > 0 \\ \langle \kappa(\mathbf{r})\kappa(\mathbf{r}')\rangle - \bar{\kappa}^2 &= (\Delta\kappa)^2 \delta(\mathbf{r}-\mathbf{r}'). \end{aligned} \tag{16}$$

There are a priori no reasons to expect any simple relation between the two fluctuating quantities and they are kept independent. Nevertheless, a simple estimate can be obtained by the capillary tube model, where $\bar{\kappa} \simeq r_0^2/12$ and $\bar{p}_c \simeq 2\sigma/r_0$ where r_0 is a typical pore radius. Although in a single pore large capillary pressure means low permeability and vice versa this simple relation is lost by coarse-graining after which one volume element contains many elementary pores. If the variation of pore size is of order δr_0 centered around a mean value $\bar{r}_0$, the variation of κ and p_c can be related as $|\Delta\kappa/\Delta p_c| \simeq 2\bar{\kappa}/\bar{p}_c$.

It is fairly easy to argue that capillary and permeability disorder act on different length scales, as was pointed out by Pauné and Casademunt [43]. To first order, the fluctuations in the permeability arise in the form

$$(\boldsymbol{\nabla}\Delta\kappa)\cdot(\boldsymbol{\nabla}p) \sim \frac{\Delta\kappa}{\xi_\kappa}\frac{\eta v}{\bar{\kappa}} \tag{17}$$

where Darcy's law has been used and ξ_κ represents a yet unknown length scale. On the other hand, fluctuations in the capillary pressure appear as

$$\bar{\kappa}\nabla^2\Delta p_c \sim \bar{\kappa}\frac{\Delta p_c}{\xi_\kappa^2}. \tag{18}$$

Equating the two terms then yields

$$\xi_\kappa \sim \frac{\bar{\kappa}^2}{\eta v}\frac{\Delta p_c}{\Delta\kappa} \sim \frac{\bar{\kappa}^{1/2}}{Ca} \tag{19}$$

where the last form assumes that permeability and capillary pressure can be written in terms of a typical capillary radius [11,43].

The most important length scale in the model is the interfacial thickness $\zeta = (K\beta)^{1/2}$. Within this scale, the concentration relaxes to the equilibrium values $c = 0$ and 1 with a rate $\sim\bar{\kappa}/(\eta\beta)$. On larger scales, the dynamics is quasistationary and dominated by the motion of the interface. It then reduces to the classical equations for fronts in porous media. The pressure field is obtained by a Laplace equation $\boldsymbol{\nabla}\cdot(\kappa\boldsymbol{\nabla}p) = 0$ with a Gibbs-Thomson-Laplace boundary condition at the interface

$$p_{\mathrm{int}} = \sigma\mathcal{K} - \bar{p}_c \tag{20}$$

where $\mathcal{K}$ is the global curvature of the imbibition front. The velocity of the interface normal to the curvature is then obtained as

$$v_n(h(\mathbf{x},t)) = \eta^{-1}\,\kappa(\mathbf{x}, h(\mathbf{x},t))\;\partial_n p(\mathbf{x}, h(\mathbf{x},t). \tag{21}$$

On length scales $l \gg \zeta$, the dynamics of the phase field approach is completely equivalent to the usual treatment of two-phase flow in porous media. It is however a lot simpler computationally, since the interface is explicitly included in the model and does not have to be tracked. Note that the model does not include trapping, any bubbles of phase $c = 0$ are eventually reduced. This is however not a problem in three dimensions, where trapping is not relevant [44], and in two dimensions, for very thin media, where air can escape from the surface on the sides.

2.2 Average height and interface equation

We explore the dynamics of the interface by first considering the behavior of the average interface height $H(t)$, i.e., we neglect all variations in the permeability and capillary pressure. Under forced imbibition, the influx of liquid is constant and so $H(t) = \gamma_0 t$, a constant progression. In spontaneous imbibition, the action of capillary forces and the solution of the Laplace equation $\nabla^2 p = 0$, with boundary condition $p(H) = -\bar{p}_c$ is

$$p(z) = -\bar{p}_c \frac{z}{H}. \tag{22}$$

The velocity is then

$$\frac{dH}{dt} = \frac{\bar{\kappa}}{\eta}\frac{\bar{p}_c}{H}. \tag{23}$$

This is the classic Lucas-Washburn result [45] and leads to an average progression $H(t) = \sqrt{2\bar{\kappa}\bar{p}_c t/\eta}$. Fluctuations of dH/dt have recently been studied and were shown to contain information about the inherent nonlocality of the interface dynamics [46]. The interface is continuously slowing down. In presence of gravity,

$$\frac{dH}{dt} = \frac{\bar{\kappa}}{\eta}\left(\frac{\bar{p}_c}{H} - \rho g\right), \tag{24}$$

which implies that there is an equilibrium height $H_g = \bar{p}_c/\rho g$ which is attained by the interface. The interface follows Lucas-Washburn behavior $H(t) \sim t^{1/2}$ until a time

$$\tau_g = \frac{\bar{\kappa}\bar{p}_c}{\eta}(\rho g)^{-2} \tag{25}$$

after which it approaches H_g exponentially $H(t) = H_g(1 - \exp(-t/\tau_g))$.

Insight into the roughening process can be obtained from an interface equation, i.e., the dynamical evolution of the imbibition front $h(\mathbf{x}, t)$. The linear equation for the Fourier component $h(\mathbf{k}, t)$ can be written in the form [11,33,35]

$$\dot{h_{\mathbf{k}}} = -\left((v + \tilde{g}) + \frac{\bar{\kappa}}{\eta}\sigma\mathbf{k}^2\right)|\mathbf{k}|\, h_{\mathbf{k}} + |\mathbf{k}|\frac{\bar{\kappa}}{\eta}\{\tilde{p}\}_{\mathbf{k}} + \frac{v}{\bar{\kappa}}\{\tilde{\kappa}\}_{\mathbf{k}} \tag{26}$$

where $v = dH/dt$ the average velocity of the interface, $\tilde{g} = \rho g\bar{\kappa}/\eta$. The first two terms on the right hand side of the equations act so as to damp the fluctuations. Notice that there are functions of the *modulus* of momenta, which come from the non-local nature of the roughening process. Disorder is introduced by the functions $\{\tilde{p}\}_{\mathbf{k}}$ and $\{\tilde{\kappa}\}_{\mathbf{k}}$ which respectively represent the Fourier transformation of capillary and permeability disorder at the interface. Since the noise term depends explicitly on the interface position, analytical solutions are extremely complicated and have been obtained only in very simplified cases. Furthermore, its linear nature may hide important non-linearities. It has also been used to study (in an approximate version) numerically roughening, by transforming back and forth between the real and Fourier space representations [47].

Nevertheless, this equation highlights the principal length scales of the problem. There is a length scale $\xi_\times$ that separates viscous and capillary damping, which was also confirmed experimentally [49], given by

$$\xi_\times^2 = \frac{\bar{\kappa}}{\eta}\frac{\sigma}{v + \tilde{g}}. \tag{27}$$

In spontaneous imbibition and in the absence of gravity, the average height $H \sim t^{1/2}$, and the velocity $v \sim t^{-1/2}$, leading to a *dynamical length scale* $\xi_\times \sim t^{1/4}$. When gravity effects are important, the correlation length $\xi_\times$ attains its maximal value at pinning (i.e., $H = H_g$). We can introduce the Bond number [13]

$$Bo = \frac{\rho g \kappa}{\sigma} \tag{28}$$

and rewrite $\xi_\times(H_p) = \kappa^{1/2} Bo^{-1/2}$. Finally, in forced imbibition, this length scale is fixed and delineates two distinct regimes of roughening.

Equation (26) also shows clearly the existence of the length scale $\xi_\kappa \sim \bar{\kappa}^2 \Delta p_c/(\eta v \Delta\kappa)$, already introduced in equation (19). Since both p_c and κ are stochastic quantities, equation (19) thus represents an average, whose particular value depends on the exact noise distribution. Nevertheless, it shows clearly that capillary disorder is most efficient on scales $l \ll \xi_\kappa$ while permeability disorder acts on scales $l \gg \xi_\kappa$. Note that the effective strength of permeability disorder is proportional to the interfacial velocity. This is of course because disorder in the pore structure can influence the invasion front only if there is motion.

3 Numerical results

We first a-dimensionalize the phase field equation (14) by rescaling distance by the interfacial width ζ ($r \to r/\zeta$) and time by the timescale $\tau = \beta\zeta^2\eta/\bar{\kappa}$ ($t \to t/\tau$). The dimensionless pressure is then

$$P(c, \mathbf{x}) = c(c-1)(2\,c-1) - \nabla^2 c - g(c)p_c(\mathbf{x}) \tag{29}$$

with the dimensionless capillary pressure $p_c\beta$. The dimensionless phase field equation

$$\frac{\partial c}{\partial t} + \gamma\boldsymbol{\nabla} c = \boldsymbol{\nabla} m \boldsymbol{\nabla} p \tag{30}$$

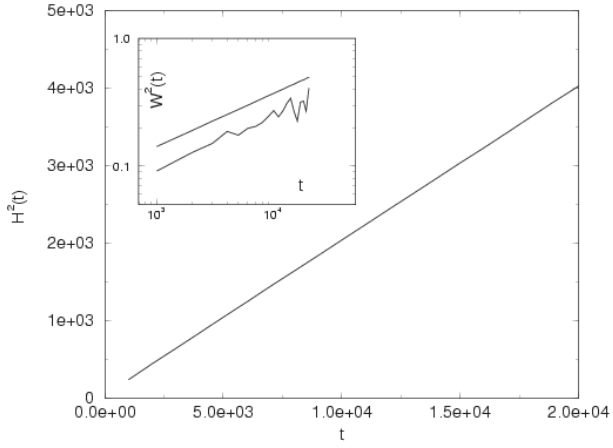

Fig. 3. Average height and width of the interface in spontaneous imbibition. The main figure shows the evolution of H^2 as a function of time. The linear behavior confirms Lucas-Washburn behavior. The inset shows the evolution of the overall width as a function of time, where power-law increase with time is observed. The straight line is a fit to the data, indicating $w^2(t) \sim t^{2\beta}$ with $2\beta = 0.41 \pm 0.03$, in accordance with the value $\beta = 0.19$ quoted in the text. The simulations were performed with $p_c = 0.2$ and $\Delta p_c = 0.2$.

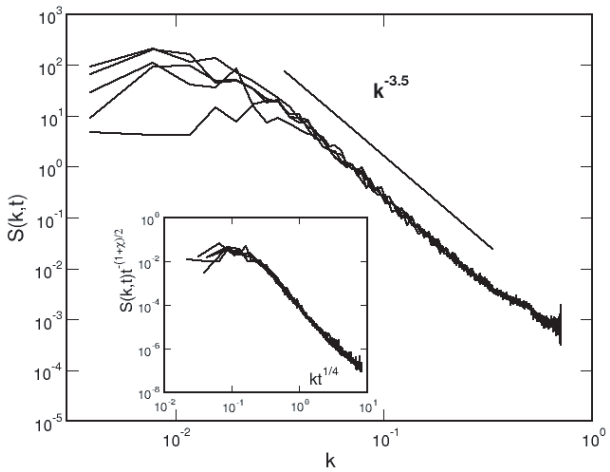

Fig. 4. Temporal evolution of the radial structure factor for spontaneous imbibition. The data show successively, from the lowest to the highest, the structure factors between $H = 5$ and $H = 40$. The insert shows the rescaling of the data with the length scale $t^{1/4}$ according to equation (31).

where the dimensionless gravity $\gamma = \rho g \beta/\zeta$ and $m = 1 + \Delta\kappa/\bar{\kappa}$. Equation (30) is then discretized on a cubic lattice using a simple finite difference scheme in space and the Euler method in time with variable time step length to avoid numerical instabilities. Higher order schemes have been used for comparison, and have brought no significant corrections to simple and fast methods. Typical simulations are made on lattices of size $L_x = L_y = 256\Delta x$ and $L_z = 150\Delta z$ with $\Delta x = \Delta z = \zeta/5$. Calculations of the width are averaged over 5 realizations of disorder while angular averages are performed in the calculations of the structure factors.

From the phase field, the interface $h(\mathbf{x}, t)$ is obtained by finding the position at which $c(\mathbf{x}, h(\mathbf{x}, t), t) = 1/2$. Overhangs, hardly present in the simulations, are systematically cut off in evaluating the interface position. In the following, we present results for spontaneous imbibition, with and without gravity, and for forced flow imbibition.

3.1 Spontaneous imbibition

We first show the numerical simulation of the phase field model for spontaneous imbibition without gravity. In this case, the interface slows down continuously and the average interface height $H(t) \sim t^{1/2}$. Since the capillary number slows down constantly, capillary disorder is the main source of roughness in the front. Figure 3 shows the result of the simulations for the average height and the global width. The average height $H(t) \sim t^{1/2}$ as predicted, while the global width of the front increases in time following $w(t) \sim t^{0.19}$. This is different from any standard roughening exponents and is due to the non-local character of the problem.

Insight into this non-locality can be gained from the study of the structure factor of the interface, shown in Figure 4 at different times. The power-law decay at large wavevectors indicate a roughness exponent $\chi_c = 0.75$, consistent with the local value of the QEW universality class [21,22].

These results can be explained by the length scale $\xi_\times(t) \sim t^{1/4}$, introduced in equation (27), as is shown in the inset of Figure 4 where the structure factor is rescaled to the universal shape

$$S(k, t) = k^{-2-2\chi_c} \mathcal{S}(k\xi_\times(t)) \tag{31}$$

with the roughness exponent $\chi_c = 0.75$ and the scaling function $\mathcal{S}(u) \sim u^{2+2\chi_c}$ if $u \ll 1$ and $\mathcal{S}(u) \sim$ const. otherwise. Using equation (6), this yields for the global width $w(t) \sim \xi_\times^{\chi_c}(t) \sim t^{0.19}$, in agreement with the numerical observation. Note that this implies that the exponent $\beta = 0.19$ is *not* a true temporal exponent. As in two-dimensional imbibition [33], the interface is correlated only up to the length $\xi_\times(t)$, and it is the dynamics of this length scale that controls the global width.

When gravity is present, there is an equilibrium height $H_g = p_c/\rho g$, which is approached exponentially after a time τ_g given in equation (25). The height $H(t)$ is described at all times by

$$H(t) + H_g \ln\left(1 - \frac{H(t)}{H_g}\right) = -\gamma t. \tag{32}$$

Using equation (24), the correlation length $\xi_\times$ can be written as

$$\xi_\times^2(H(t)) = \frac{\sigma H(t)}{p_c} \tag{33}$$

where $H(t)$ is given by the solution of equation (32). We have already shown that at pinning, the length scale $\xi_\times(H_g) = (\bar{\kappa}/Bo)^{1/2}$. Percolation theory, for imbibition

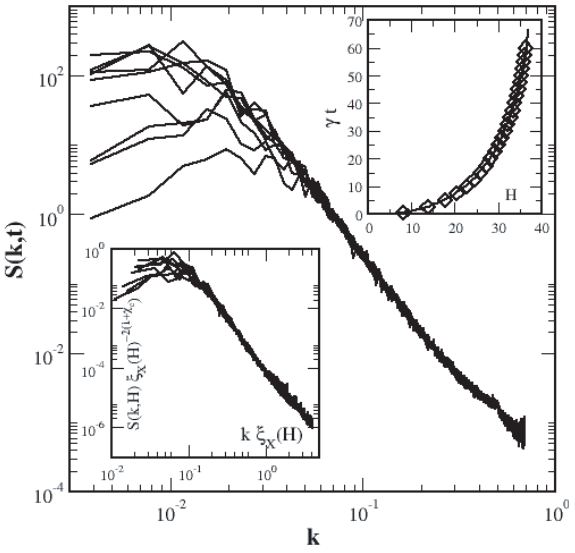

Fig. 5. Dynamical evolution of the imbibition front in presence of gravity. The main plot shows the radial structure factor for height $H = 5$ (lowest curve) to $H \approx 35$ (highest curve) for parameters $\gamma = 2.5 \times 10^{-3}$. The inset in the upper right corner shows time versus the average interface height. The numerical simulation (diamonds) compares favorably to the analytical form equation (32), drawn as a solid line. The lower inset shows the scaling of the structure factor at different heights according to equation (34).

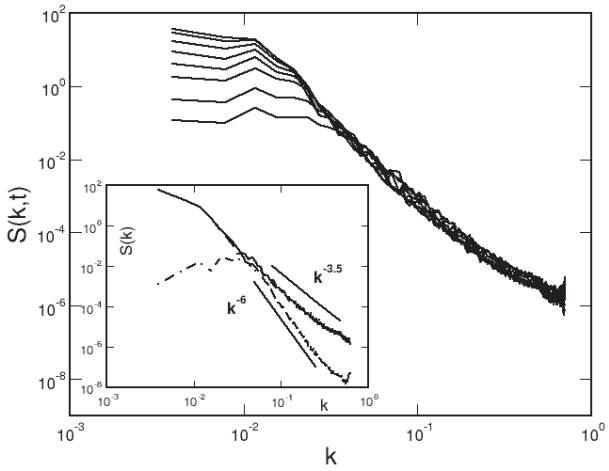

Fig. 6. Temporal evolution of the radial structure factor of an interface for which both capillary and permeability disorder is relevant. The numerical simulations were performed with $\Delta p_c/\bar{p}_c = 0.1$ and $\Delta\kappa/\bar{\kappa} = 0.5$. There is a complex interplay between both types of noise, as exposed in the inset, where it is shown that the structure factor is composed by the sum of the individual effects of capillary (with power law tail $\sim k^{-3.5}$) and permeability ($\sim k^{-6}$) disorder.

at very low capillary numbers, introduces a similar length scale $\xi_p \sim Bo^{-\gamma}$ where $\gamma = 0.47$ in two dimensions [48] and $\gamma = 4/7$ in three dimensional imbibition [50]. For all practical purposes, this is indistinguishable from our results, valid in both 2 and 3 dimensions. Of course, the dynamical approach to pinning is different from percolation theory. Figure 5 shows the dynamical evolution of the structure factor as a function of time until pinning, and we can establish the scaling form

$$S(k,t) \equiv S(k,H(t)) \sim \xi_\times^{2+2\chi_c} \mathcal{S}(k\xi_\times(H(t))) \qquad (34)$$

where again $\chi_c = 0.75$ and the scaling function similar to the scaling function of spontaneous imbibition, equation (31). The only difference is now that $\xi_\times(t) = \xi_\times(H)$ is not a power law in time anymore.

3.2 Forced flow imbibition

In forced flow imbibition, the interface moves at the constant velocity $H(t) = \gamma_0 t$ where γ_0 is the imposed flux. In this case, we expect that the length scale $\xi_\times = (\bar{\kappa}\sigma/\gamma_0\eta)^{1/2} = (\bar{\kappa}/Ca)^{1/2}$, a fixed value that limits the range of fluctuations. In addition, the capillary number is not necessarily small and we expect both capillary and permeability disorder to be relevant. The length scale ξ_κ should then become apparent in the roughness spectrum. Figure 6 shows the evolution of the structure factor for an interface where both capillary and permeability disorder are present. Although it is clear that the roughness of the interface is cut off at a given length scale, the tail of the power spectrum shows a curvature which prevent a clear identification of a roughness exponent.

This complex behavior can be explained by considering separately the effect of capillary and permeability disorder, schematically shown in the inset of Figure 6. We first perform simulations where only capillary disorder is present. Figure 7 shows the power spectrum of the saturated interface for various pressure gradients, with only capillary noise present. As in spontaneous imbibition, capillary disorder gives an interface that has the roughness exponent $\chi_c = 0.75$ within a range $l \ll \xi_\times$ while being flat asymptotically. The length $\xi_\times \sim v^{-1/2}$ now has a fixed value and the inset of Figure 6 shows that the structure factor of the saturated interface can be written as

$$S(k,t) = k^{-2-2\chi_c} \mathcal{S}(kv^{-1/2}) \qquad (35)$$

where $\mathcal{S}(u)$ has also the same scaling as spontaneous imbibition, given after equation (31).

We then examine the structure factor of a saturated interface where only permeability disorder is present, as shown in Figure 8. Immediately apparent is the velocity dependence of the amplitude of the structure factor. This is consistent with the presence of the factor of v multiplying the noise term in equation (26). The roughness exponent $\chi_\kappa \approx 2$, meaning that the interface is superrough, as is also the case in two dimensions [11,37,47]. Notice however that the amplitude of the fluctuations is extremely reduced compared to the fluctuations caused by capillary disorder. The length scale $\xi_\times$ still cuts off the large scale fluctuations and the data can now be collapsed to the common form

$$S(k,t) = v^2 k^{-2-2\chi_\kappa} \mathcal{S}(kv^{-1/2}) \qquad (36)$$

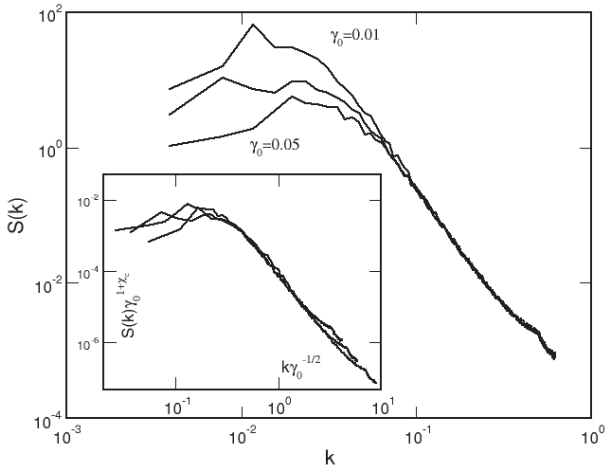

Fig. 7. A log-log plot of the radial structure factor for saturated interfaces in forced flow imbibition when only capillary disorder is present. The various curves represent different pressure gradients γ_0 (from top to bottom) $\gamma_0 = 0.01, 0.05$ and 0.1. The decay of the structure factor still indicates a fractal surface, with roughness $\chi = 0.75$. The fractal character is again cut off at a given length scale, but this time, it has a fixed value $\xi_\times \sim \gamma_0^{-1/2}$. The inset shows the rescaling of the data with velocity to the universal form of equation (35).

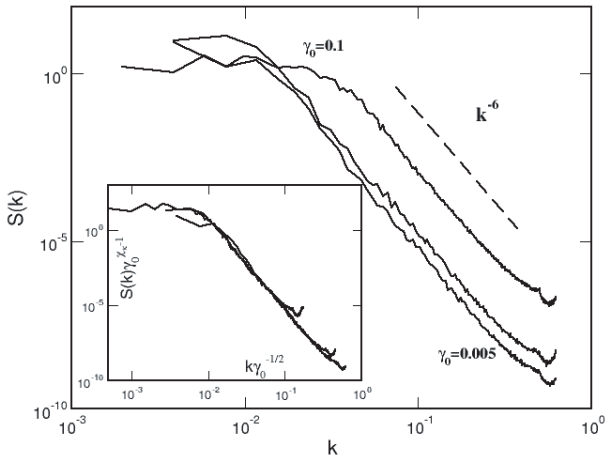

Fig. 8. Radial structure factor of a saturated interface when only permeability disorder is present. The numerical simulations were performed with $\gamma_0 = 0.005, 0.01$ and 0.1, with $\Delta\kappa/\bar{\kappa} = 0.5$. The inset shows the rescaling of the data based on the length scales $\xi_\times \sim \gamma_0^{-1/2}$.

where the exponent $\chi_\kappa \approx 2$ and the scaling function $s(u)$ given after equation (31).

When both capillary and permeability disorder are present, the length scale ξ_κ separates the influence of capillary and permeability noise, as shown in the inset of Figure 6. Capillary disorder, gives the main contribution to roughness on short scales $k > \xi_\kappa^{-1}$ while permeability disorder roughens the opposite regime. The complete spectrum then results from the superposition of both types of disorder, being cutoff on length scales larger than $\xi_\times$.

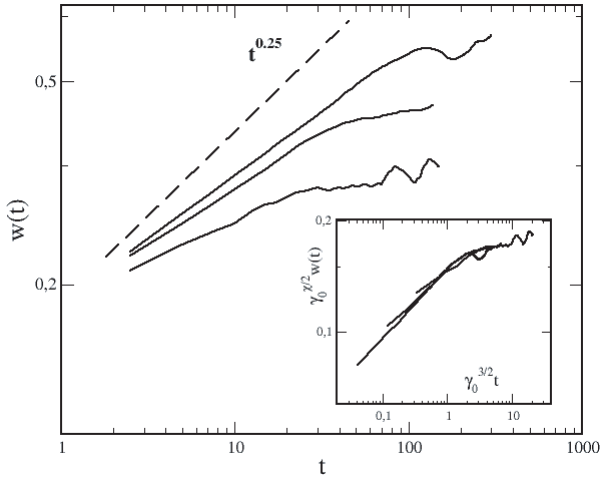

Fig. 9. Time evolution of the interfacial width for various pressure gradients $\gamma_0 = 0.067, 2\gamma_0$ and $4\gamma_0$, respectively from top to bottom. The faster interface has a smaller total roughness. In order to get reliable data, the simulations must be performed with lattice spacing $\delta = 0.75\zeta$ and $dt = 0.0025$. The initial slope of $w(t)$ is smaller than the value $\beta = 0.25$ expected theoretically, but the rescaling of the data to the common form equation (37), shown in the inset confirms our predictions

To study the dynamics of the fluctuations, we concentrate on the low capillary number regime, where only capillary disorder is relevant. Based on the linearized interface equation, equation (26), we expect early time roughening to be dominated by a dynamical exponent $z = 3$, as was found in two dimensions by Soriano et al. [51]. So there should be a correlation length $\xi_3(t) \sim (\sigma t)^{1/3}$ such that $w(t) \sim \xi_3^{\chi_c} \sim t^\beta$. With the value $\chi_c = 0.75$, this then gives $w(t) \sim t^{\chi_c/3} \sim t^{0.25}$. This behavior should persist until a time $t_\times$ such that $\xi_3(t_\times) = \xi_\times$, which implies $t_\times \sim v^{-3/2}$.

The numerical simulations show that the saturation of the width is extremely rapid, and it is therefore difficult to obtain reliable data. The initial slope of the width is always systematically smaller than the expected value of 0.25 and indicates a very gradual approach to saturation. At later times, the width flattens out, to an effective exponent (only defined on the small window available) $\beta \approx 0.1$, more representative of logarithmic roughening than true power-law behavior, a trend confirmed by the form of the structure function. For all practical purposes, the inset of Figure 9 shows that the dynamical width of the interface obeys the scaling form

$$w(t) = \xi_\times^{\chi_c} \omega(t/t_\times) \tag{37}$$

where $\omega(u) \sim u^{\chi_c/3}$ for times early times $t \ll t_\times$. This is the standard scaling equation for the dynamical width, with initial power law $w(t) \sim t^{\chi_c/0.3}$ saturating to a fixed value $w(t \gg t_\times) \sim \xi_\times^{\chi_c}$ at times much larger than the crossover time $t_\times \sim v^{-3/2}$. The linearized equation also predicts the existence of a time scale $\xi_1 \sim vt$. The time development of the width is determined by the ξ_3 term as long as $\xi_3 \ll \xi_\times$ while the slower ξ_1 is only effective at times when $\xi_1 \ll \xi_\times$. It is thus possible to add a correction

term to the scaling function $\omega(u \gg 1) \sim \text{const.} + \mathcal{O}(\log u)$. But again, we must emphasize that this behavior is very difficult to see numerically.

4 Experimental implications

We now discuss some important implications of our results. We will focus on the hindsight that our approach, mid-way between the full complexity of the network simulations and the simplified one-dimensional treatment may bring. We also concentrate on flows at low capillary numbers, so that capillary disorder is dominant.

First, we present the dynamics of the global concentration $\mathcal{C}(z)$, defined as the spatial average of the local concentration over the front

$$\mathcal{C}(z) = \overline{\theta(h(\mathbf{x},t) - z)}. \tag{38}$$

where the function $\theta(x) = 1$ if $x \geq 0$ and $\theta(x) = 0$ is $x < 0$. Because the interface separating the wet and dry phase of the medium is a self-affine fractal [52], this is a well-defined quantity, with limits $\mathcal{C}(0) = 1$ and $\mathcal{C}(z \to \infty) = 0$. The transition between these two values occurs over a region of width $w(Ca)$, the roughness of the two-dimensional interface at capillary number Ca. Assuming that the interface has Gaussian fluctuations, it is indeed straightforward to show that [52]

$$\mathcal{C}(z) = \int_z^\infty D[h]P[h] \equiv \text{erfc}\left(\frac{z - H_0(t)}{w(t)}\right) \tag{39}$$

where $P[h] \sim \exp(-h^2/w^2)$ represents the Gaussian probability of the fluctuations and $\text{erfc}(z)$ is the complementary error function. This then presents the picture of imbibition as the progression of an average front becoming more and more spread out as time goes by. In spontaneous imbibition, the front has average progression $H(t) \sim t^{1/2}$ and is spread over a length $w(t) \sim t^{\chi_c/4}$. In forced imbibition, the average front progresses at constant velocity while its width increases like $t^{\chi_c/3}$ until it reaches the saturated value $w \sim Ca^{-\chi_c/2}$. Note that this picture of a one-dimensional front with time varying width is a common feature of Richard's Equation and experiments of imbibition that look at the global average features of the front, such as NMR and capillary fringes phenomena [15].

Another important application of the results presented above is fluid breakthrough across a thin porous medium such as a membrane, a paper sheet or a coating layer. In spontaneous imbibition, if H_0 is the thickness of the layer, then the average time needed for breakthrough is $T_0 = \eta H^2/\kappa p_c$. However, due to the disordered structure of the medium, the breakthrough is not uniform but takes place by "patches", as shown in Figure 2. Since at height H_0, the interface has global roughness $w_0 \sim H_0^{\chi/2}$, the time it takes for completing breakthrough is $\Delta T \sim \Delta(H_0^2) \sim w_0 H_0 \sim H_0^{1+\chi/2}$. If the flow of liquid is forced with some flux γ_0, then the range of the fluctuations is limited by the length $\xi_\times \sim (\sigma/\gamma_0)^{1/2}$ and breakthrough is completed after a time $\Delta T = \xi_\times^\chi/\gamma_0 \sim \gamma_0^{-1-\chi/2}$.

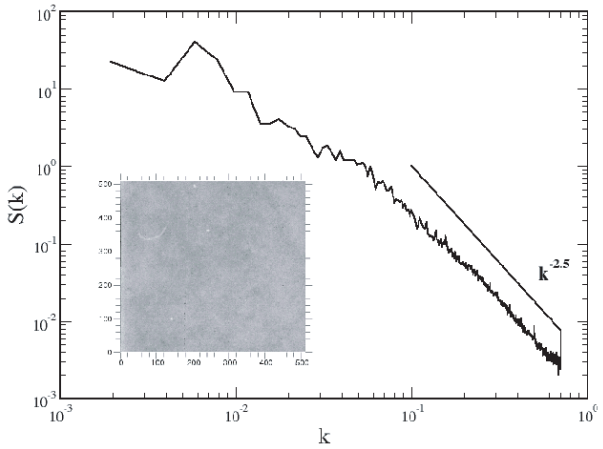

Fig. 10. Spatial structure of light intensity through a partially wet sheet of paper (Fig. 2). The inset shows the interface $h(\mathbf{x},t)$ according to equation (41) while the main figure depicts its structure factor and clearly shows self-affine behavior (roughness exponent $\chi \approx 0.25$ at large wavevectors. The complex structure of paper cannot be treated within the simple model presented here, but the figure nevertheless illustrates that the concepts of dynamical roughening can be applied to this case.

The structure of the patches is also connected to the roughness of the underlying interface. We define the patches as $\chi(\mathbf{x},t) = \theta(h(\mathbf{x},t) - H_0(t))$, the fluctuations of the rough interface $\delta h(\mathbf{x},t) = h(\mathbf{x},t) - H_0(t)$ around the mean, and the associated correlation function

$$\mathcal{G}(\mathbf{x},\mathbf{x}',t) = \langle \chi(\mathbf{x},t)\chi(\mathbf{x}',t)\rangle. \tag{40}$$

A simple expansion to first order yields $\mathcal{G} \sim \langle \delta h(\mathbf{x},t)\delta h(\mathbf{x}',t)\rangle$, with Fourier transform $\langle |\delta h(\mathbf{k},t)|^2\rangle \sim S(\mathbf{k},t)$, the structure factor given in equations (31, 34) and (36) for the various cases considered in this paper. Referring to Figure 2, Figure 10 shows the structure factor of the quantity

$$\ln \frac{I(\mathbf{x},t)}{I_0(\mathbf{x})} \sim \gamma h(\mathbf{x},t), \tag{41}$$

which, assuming an exponential relation between local height and light intensity, corresponds to the interfacial height of the wetting front. It is clear that in this particular case, the propagation of the front is influenced by phenomena such as dynamical swelling of the fiber or diffusion of water through the fiber, and the wetting front is to some extent correlated with the height and density fluctuations (often referred to as the "formation" of the sheet). Finite size effects are also important in this particular experiment [53], but it is clear that the structure factor shows a crossover to a self-affine factor at small length scales. Dynamical wetting of the paper structure could then be approached by extending the method exposed in the paper along the lines explored in reference [54]. This is however beyond the scope of this work.

5 Conclusion

We have explored front roughening of a fluid-gas interface in a three-dimensional disordered solid. The following generic features have already been studied in the two-dimensional case. The pore structure gives rise to two types of disorder: capillary disorder, acting specifically at the interface, and permeability disorder, related to the overall flow of liquid. Permeability and capillary disorders act on different length scales. On short length scales, capillary disorder is stronger while permeability disorder dominates on larger length scale. On the scales for which capillary disorder is dominant, the interface in three dimensions has roughness exponent $\chi_c = 0.75$ while the roughness the interface on larger length scales is super-rough. The interplay between fluid conservation and surface tension gives rise to the length scale $\xi_\times = (\sigma/v)^{1/2} \sim Ca^{-1/2}$, which separates two regimes of roughness. The effect of this length scale is most apparent in spontaneous imbibition, where the effect of permeability disorder is less important. In such a case, the interface has roughness exponent χ_c on scales smaller than $\xi_\times$ while being flat asymptotically. In addition spontaneous imbibition is characterized by an interface that is continually slowing down, leading to a time-dependent cutoff length scale $\xi_\times = \xi_\times(t) \sim t^{1/4}$. This results in a time increase of the width of the interface $w(t) \sim \xi_\times^{\chi_c}(t)$ described by an effective dynamical exponent $\chi_c/4$. In forced imbibition, capillary disorder is again dominant for flows with a small capillary number. In this case, the length scale $\xi_\times$ is constant in time. The interface still has a roughness exponent χ_c on scales smaller that $\xi_\times$, while being much smoother on large scales. The initial dynamical increase of the width is now given in terms of the exponent $\beta = \chi_c/3$, corresponding to the exponent $z = 3$.

Finally, our results on three-dimensional roughening of interfaces can be applied in several situations of fluid penetration in porous media. One example is given by the fluctuations Δv of average interface velocity $\bar{v}$ [46], implying that $\Delta v \sim \bar{v}^{1/2}$ for a spontaneously rising column of fixed width under the influence of dominant capillary disorder. The roughness of the front is also of practical interest as highlighted by the study of water fronts referred to in Sections 1 and 4. This clearly shows the need for more systematic experiments.

Fruitful and intensive discussions with J. Lohi are gratefully acknowledged. The Academy of Finland is thanked for support (Center of Excellence program), as well as KCL Ltd.

References

1. M.I.J. van Dijke, K.S. Sorbie, J. Pet. Sci. Eng. **39**, 201 (2003)
2. J. Rosinski, Am. Ink Maker **71**, 40 (1993)
3. J. Aspler, Nordic Pulp Paper Res. J. **1**, 68 (1993)
4. N. Poulin, P. Tanguy, J. Aspler, L. Larrondo, Can. J. Chem. Eng. **75**, 949 (1997)
5. C.J. Ridgway, P.A.C. Gane, Nordic Pulp Paper Res. J. **17**, 119 (2002)
6. M.J. Blunt, M.D. Jackson, M. Piri, P.H. Valvatne, Adv. Water Resour. **25**, 1069 (2002)
7. A. Leventis, D.A. Verganelakis, M.R. Halse, J.B. Webber, J.H. Strange, Transp. Porous Media **39**, 143 (2000)
8. J.S. Ceballos-Ruano, T. Kupka, D.W. Nicoll, J.W. Benson, M.A. Ioannidis, C. Hansson, M.M. Pintar, J. Appl. Phys. **91**, 6588 (2002)
9. N.M. Abboud, Transp. Porous Media **30**, 199 (1998)
10. W. Hwang, S. Redner, Phys. Rev. E **63**, 021508 (2001)
11. M. Alava, M. Dubé, M. Rost, Adv. Phys. **53**, 83 (2004)
12. R. Lenormand, J. Phys. Cond. Mat. **2**, SA79 (1990)
13. M. Sahimi, Rev. Mod. Phys. **65**, 1393 (1993)
14. A.M. Tartakovsky, S.P. Neuman, R.J. Lenhard, Phys. Fluids **15**, 3331 (2003)
15. D. Ronen, H. Scher, M.J. Blunt, Trans. Porous Media **28**, 159 (1997)
16. R.G. Hughes, M.J. Blunt, Trans. Porous Media **40**, 295 (2000)
17. E. Aker, K.J. Maloy, A. Hansen, Phys. Rev. E **61**, 2936 (2000)
18. M Dubé, F. Mairesse, J.P. Boisvert, Y. Voisin, Submitted, IEEE Trans. Image Analysis (2005)
19. A.-L. Barabási, H.E. Stanley, *Fractal Concepts in Surface Growth* (Cambridge University Press, Cambridge, 1995)
20. M. Dubé, B. Chabot, C. Daneault, M. Alava, Pulp & Paper Canada **106**, 24 (2005)
21. H. Leschhorn, T. Nattermann, S. Stepanow, L.-H. Tang, Ann. Physik **6**, 1 (1997)
22. J.M. Schwarz, D.S. Fisher, Phys. Rev. E **67**, 021603 (2003)
23. S.V. Buldyrev, S. Havlin, H.E. Stanley, Physical A **200**, 200 (1993)
24. A. Rosso, W. Krauth, Phys. Rev. Lett. **87**, 187002 (2001)
25. J. Bear, Y. Bachmat, *Introduction to modeling of transport phenomena in porous media* (Kluwer Academic, Dordrecht, 1991)
26. T.J. Senden, M.A. Knackstedt, M.B. Lyne, Nordic Pulp Paper Res. J. **15**, 554 (2000)
27. C.J. Ridgway, P.A.C. Gane, J. Schoelkopf, J. Coll. Int. Sci. **252**, 373 (2002)
28. D.E. Eklund, P.J. Salminen, Tappi Journal **69**, 116 (1986)
29. L.A. Richard, Physics (N.Y.) **1**, 318 (1931)
30. J. Asikainen, S. Majaniemi, M. Dubé, J. Heinonen , T. Ala-Nissila, Eur. Phys. J. B **30**, 253 (2002)
31. R. Chandler, J. Koplik, K. Lerman, J.F. Willemsen, J. Fluid. Mech. **119**, 249 (1982)
32. C.-H. Lam, V.K. Horváth, Phys. Rev. Lett. **85**, 1238 (2000)
33. M. Dubé, M. Rost, K.R. Elder, M. Alava, S. Majaniemi, T. Ala-Nissila, Phys. Rev. Lett. **83**, 1628 (1999)
34. M. Dubé, M. Rost, M. Alava, Eur. Phys. J. B **15**, 691 (2000)
35. M. Dubé, M. Rost, K.R. Elder, M. Alava, S. Majaniemi, T. Ala-Nissila, Eur. Phys. J. B **15**, 701 (2000)
36. M. Dubé, S. Majaniemi, M. Rost, K.R. Elder, M. Alava, T. Ala-Nissila, Phys. Rev. E **64**, 051605 (2001)
37. A. Hernández-Machado, J. Soriano, A.M. Lacasta, M.A. Rodríguez, L. Ramírez-Piscina, J. Ortín, Europhys. Lett. **55**, 194 (2001)
38. I. Mitkov, D.M. Tartakovsky, C.L. Winter, Phys. Rev. E **58** R5245, (1998)
39. P. Papatzacos, Trans. Porous Media **49**, 139 (2002)

40. This compressibility arises from the finite curvature of the potential wells but only introduces a minor perturbation. On long time scales, the fluid is essentially incompressible, cf., the discussion above equation (4)
41. J. Soriano, J.J. Ramasco, M.A. Rodríguez, A. Hernández-Machado, J. Ortín, Phys. Rev. Lett. **89**, 026102 (2002)
42. D. Jasnow, J. Viñals, Phys. of Fluids **7**, 747 (1996)
43. E. Pauné, J. Casademunt, Phys. Rev. Lett. **90**, 144504 (2003)
44. D. Wilkinson, J.F. Willemsen, J. Phys. A: Math. Gen. **16**, 3365 (1983)
45. E.W. Washburn, Phys. Rev. **17**, 273 (1921)
46. M. Rost, L. Laurson, M. Dubé, M. Alava, Phys. Rev. Lett. **98**, 054502 (2007)
47. T. Laurila, C. Tong, S. Majaniemi, I. Huopaniemi, T. Ala-Nissila, Eur. Phys. J. B **46**, 553 (2005)
48. D. Wilkinson, Phys. Rev. A **34**, 1380 (1986)
49. D. Geromichalos, F. Mugele, S. Herminghaus, Phys. Rev. Lett. **89**, 104503 (2002)
50. J.-F. Gouyet, B. Sapoval, M. Rosso, Phys. Rev. B **37**, 1832 (1988)
51. J. Soriano, A. Mercier, R. Planet, A. Hernández-Machado, M.A. Rodríguez, J. Ortín, Phys. Rev. Lett. **95**, 104501 (2005)
52. See e.g., R. Kant, Phys. Rev. E **53**, 5749 (1996). For a self-affine interface, the the roughness exponent, $\chi < 1$, leads to $w(L)/L \to 0$ asymptotically at large distances. This implies that $\mathcal{C}(z) \sim e^{-z/w}$. The result equation (39) is for the special case of an interface with Gaussian fluctuations.
53. V. Vuorinen, HUT project report (2003)
54. J. Ketoja, K. Niskanen, in *12th Fundamental Research Symposium* (Oxford, 2001)